IEEE Journal of Microwaves

Received 22 March 2022; revised 29 April 2022; accepted 12 May 2022. Date of publication 13 June 2022; date of current version 7 July 2022.

Digital Object Identifier 10.1109/JMW.2022.3175625

Reconfigurable Liquid Crystal Dielectric Image Line Leaky Wave Antenna at W-Band

HENNING TESMER, RANI RAZZOUK, ERSIN POLAT, DONGWEI WANG (Graduate Student Member, IEEE), AND ROLF JAKOBY (Member, IEEE)

(Regular Paper)

Institute of Microwave Engineering and Photonics, Technische Universität Darmstadt, 24289 Darmstadt, Germany

CORRESPONDING AUTHOR: Henning Tesmer (e-mail: henning.tesmer@tu-darmstadt.de).

This work was supported by Deutsche Forschungsgemeinschaft (DFG) under Project 398656024, and the Open Access Publishing Fund of the Technical University of Darmstadt.

ABSTRACT This paper presents a reconfigurable dielectric image line leaky wave antenna at W-band. Reconfigurability is achieved by applying bias to anisotropic liquid crystal (LC) filled into the antenna. Instead of separating RF components and DC-bias network by complex or space consuming methods, the bias electrodes are simultaneously used as radiation elements. In order to evaluate this concept, a non-reconfigurable antenna with isolated unit cells is compared to a reconfigurable antenna, which has its unit cells connected by a metallic line. The non-reconfigurable demonstrator shows gain of up to 18 dBi and can scan through broadside from -30° to $+10^\circ$ in the investigated frequency range from 75 GHz to 102 GHz. This frequency scanning sector can be shifted by 10° when utilizing the reconfigurable LC antenna, while gain of up to 15 dBi is maintained. Since the bias electrodes are directly mounted on the image line, less than 50 V is necessary to control the LC. The antenna is comparably easy to fabricate, and only one bias voltage is directly related to a steering angle, which can be advantageous compared to complex phased arrays with multiple LC phase shifters.

INDEX TERMS Beam steering, dielectric image line, leaky wave antennas, liquid crystal, W-band.

I. INTRODUCTION

The ever rising demand of high data rate in wireless applications, such as autonomous sensor/machine networks, remote sensing and positioning, radar imaging or point-to-point communication forces future wireless systems to utilize upper millimeter-wave (mmW) frequencies. Along with the benefit of higher achievable absolute bandwidths comes the challenge of increased free space loss and propagation loss in conventional planar waveguide topologies such as microstrip or coplanar waveguides. In order to compensate free space loss, high gain aperture antennas or arrays of antennas have to be employed. The necessary high gain results in a narrow beam, which can make precise alignment of transmitter and receiver challenging, especially in non-stationary environments. Therefore, beam steering is necessary either to track a moving transceiver, or to compensate small misalignment of transmitter and receiver in (semi-)stationary scenarios. In general, electrical beam steering is preferred to moving the whole antenna, e.g. by a motor, since the necessary mechanical components consume space and have to be maintained. Hence, electrically reconfigurable components are employed [1] such as micro-electromechanical systems (MEMS) [2], semiconductors [3], barium strontium titanate (BST) [4], [5], and liquid crystal (LC) [6]. At higher mmW frequencies, semiconductors and BST show increased loss. While MEMS certainly show good performance, they are still mechanical systems which can lead to wear-out failures. As an all electrical, continuous tunable alternative, this work utilizes LC. Controlling the orientation of the anisotropic, rod-like LC molecules with respect to the RF-field by an applied electro- and/or magnetostatic bias field, leads to different permittivity and loss tangent. Thus, between the two extreme alignment cases, i.e. parallel alignment with $\varepsilon_{r,||}$ and $\tan\delta_{||}$ and perpendicular alignment $\varepsilon_{r,\perp}$ and $\tan\delta_{\perp}$, continuous tuning is possible. It could be observed that LC shows stable material properties up to the Terahertz regime [6]. Therefore, the

concepts introduced in this paper could be extended to higher frequency ranges. LC has been employed in various topologies in order to achieve reconfigurable components. At mmW, LC-filled dielectric waveguides (DWGs) have been investigated to provide low-loss reconfigurable components [7]. While showing good performance, the demonstrators have limitations due to increased response time and bulky bias networks. Since the bias electrodes have to maintain a minimum distance to the DWG such that the evanescent field components of the DWG are not disturbed, it is challenging to implement large phased arrays. Hence, the advantage of high freedom in beam forming obtained with a phased array is paid by growing complexity of power distribution and bias control network for phase shifters. This paper tackles this problem by two ways: First, the bias electrodes are deliberately accepted to radiate, i.e. they are both used as a radiation element as well as a bias element, hence, forming a leaky wave antenna (LWA). Second, instead of the waveguide topology being fully dielectric, which is hard to integrate to any conventional printed circuit board (PCB), the dielectric image line (DIL) topology is utilized [8], [9]. This topology proved to be advantageous not only due to its quasi-planar structure, but also with regard to faster response time when compared to fully dielectric structures [10]. Since the electrodes are meant to be put directly on the DIL hosting the LC, a reconfigurable LWA with low fabrication complexity can be realized. LWAs have been investigated in various frequency ranges and many waveguide topologies, including the DIL topology [11]–[17]. They offer a simple, low-cost way to achieve directive patterns which are scanned with changing the operation frequency. Due to their simplicity, a complex feed network can be avoided, which lowers total loss. This is especially important in the mmW regime, in which various DIL-LWAs have been proposed, and different techniques to circumvent common problems such as an open-stopband have been investigated in the past years [18]–[22]. Reconfigurable LWAs can be realized with various technologies, including LC [23]–[28]. However, many LC-LWAs are investigated solely in an analytical or simulative manner. In general, the frequency scanning behavior of an LWA might exclude the use for communication. However, moving to higher frequencies of operation and utilizing lower permittivity dielectrics in order to avoid fast scanning [29] can provide larger absolute bandwidth for a certain frequency-angle pair. The principle of the antenna proposed in this paper is sketched in Fig. 1. The frequency scanning sector can be shifted when changing the permittivity of the LC embedded in the antenna body. The remainder of this paper is organized as follows: in Section II, DIL leaky wave antenna fundamentals are covered, before the investigated unit cells and the general layout of the antenna are proposed in Section III. Fabrication and measurement results are presented in Section IV, and the paper concludes with a summary and outlook in Section V.

II. DIELECTRIC IMAGE LINE LEAKY WAVE ANTENNAS

The DIL topology has been used to create LWAs of different permittivity with different scanning capabilities at various

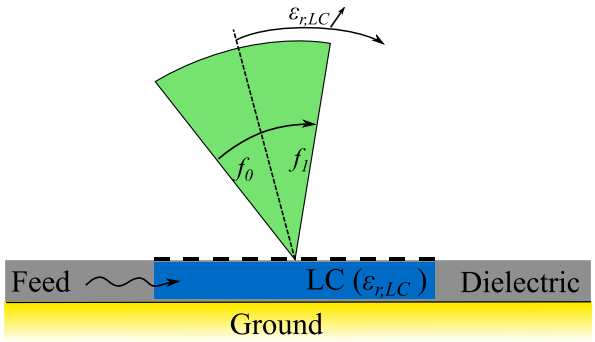

FIGURE 1. Depending on the LC permittivity inside the DIL-LWA, the sector covered by sweeping the frequency from f_0 to f_1 can be steered. Since LC can be continuously tuned between its minimum ($\epsilon_{r,\perp}$) and maximum ($\epsilon_{r,||}$) permittivity, continuous tuning of the sector is possible.

frequencies [16], [20], [30]–[35]. A rectangular DIL with fixed aspect ratio of $a = 2 \cdot b$, where a denotes its width and b its height, operates in single mode with good confinement of the field if

$$b \approx \frac{0.32\lambda_0}{\sqrt{\varepsilon_r - 1}}, \tag{1}$$

where λ_0 is the free space wavelength and ϵ_r is the permittivity of the dielectric [36]. In this paper, the used dielectric is Rexolite 1422 with $\varepsilon_r = 2.53$ and $\tan\delta = 6 \cdot 10^{-4}$ at 94 GHz [37]. For operation from 75 GHz to 110 GHz (W-band), a height of $b = 0.9$ mm and therefore, a width of $a = 1.8$ mm is chosen.The scanning angle θ of an LWA can be approximated by

$$\theta \approx \sin^{-1}\left(\frac{\beta(\omega)}{k_0}\right), \tag{2}$$

where $\beta(\omega)$ denotes the propagation constant in z and k_0 the free space propagation constant. In this paper, only 1D periodic LWAs are investigated. With the help of Floqet's Expansion and the consideration of spatial harmonics, Brillouin Dispersion Diagrams are calculated in order to predict the LWAs' properties. For that, the guided mode is represented by an infinite number of n space harmonics [29]:

$$k_{z,n} = k_{z,0} + \frac{2\pi n}{p} = \beta_n - j\alpha, \tag{3}$$

$$\beta_n = \beta_0 + \frac{2\pi n}{p}. \tag{4}$$

α denotes the leakage constant, β_n represents the n-th propagation constant, and p describes the unit cell length, i.e. the spatial period. The relation of propagation constants and radiation angle (c.f. eq 2) are visualized for the unit cells with the help of Brillouin Diagrams in Section III. Usually, the $n = -1$ space harmonic is used for the radiative behavior. Since the dielectric (Rexolite, $\varepsilon_r = 2.53$) is chosen such that it fits to the LC's permittivity range ($\varepsilon_r = 2.46$ to 3.53), no full forward to backward scan is possible without grating lobes [29], [38]. However, due to the resulting slow scan with frequency, larger bandwidths per scanning angle are achievable.

TABLE 1. Dimensions of the Unit Cells Shown in Fig. 2

Parameter	a	b	p	l_s	l_t	w_s	w_l	t	w_{conn}	w_{LC}	h_{LC}
Value (mm)	1.8	0.9	2.3	0.7	1.5	1.5	0.3	0.009	0.075	1.25	0.8

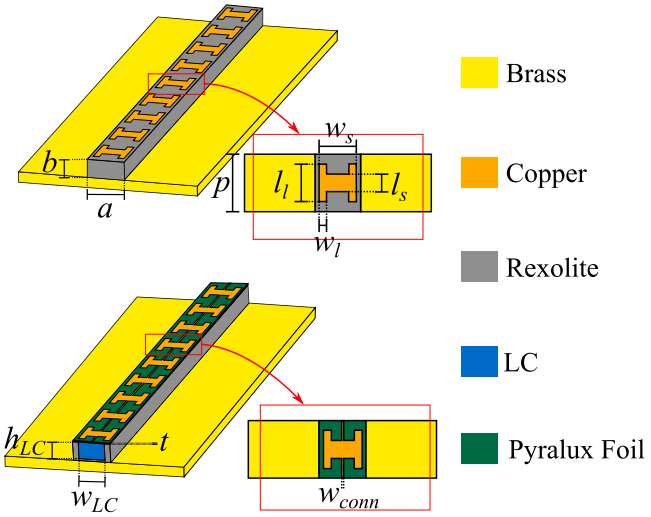

FIGURE 2. Antenna layouts with a zoomed view to the unit cells. Top: non-reconfigurable LWA with pure Rexolite body. Bottom: reconfigurable LWA with LC cavity sealed by Pyralux foil. Dimensions are given in Table 1.

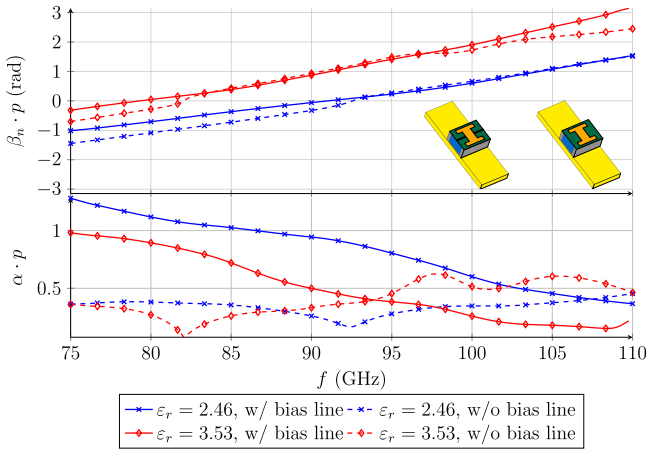

FIGURE 3. Dispersion diagrams showing the characteristics of phase constant β (top) and leakage constant α (bottom) for both unit cells with and without a bias line, considering both highest and lowest possible LC permittivity. Representations of the unit cells are included as insets in the plot.

III. UNIT CELL AND ANTENNA DESIGN

The investigated LWAs with and without an LC cavity below are depicted in Fig. 2. Corresponding dimensions are given in Table 1. The unit cell should both (1.) act as a radiation element and (2.) simultaneously provide proper bias to the LC medium. Therefore, a geometry is required, which covers as much of the LC cavity as possible, while also being able to suppress an open-stopband. H-shaped unit cells fulfill both requirements [20]. Their final dimensions are optimized with CST Studio Suite. The LC mixture used in this work is GT7-29001 from Merck KGaA, Darmstadt, Germany with following parameters given at 19 GHz: $\varepsilon_{r,||} = 3.53$, $\varepsilon_{r,\perp} = 2.46$, $\tan\delta_{||} = 0.0064$ and $\tan\delta_{\perp} = 0.0116$ [39]. Therefore, the dielectric anisotropy of the material is $\Delta\varepsilon_r = \varepsilon_{r,||} - \varepsilon_{r,\perp} = 1.07$. The propagation constant β and leakage constant α of a structure with infinite unit cells can be determined by [40]

$$\beta_n p = \left|\mathrm{Im}\left(\cosh^{-1}\left(\frac{1 - S_{11}S_{22} + S_{21}S_{12}}{2S_{21}}\right)\right)\right| \quad (5)$$

$$\alpha p = \left|\mathrm{Re}\left(\cosh^{-1}\left(\frac{1 - S_{11}S_{22} + S_{21}S_{12}}{2S_{21}}\right)\right)\right|, \quad (6)$$

when investigating a single cell. The bias line connecting the H-shapes contributes to the radiative behavior, as Fig. 3 illustrates. Especially at lower frequencies, the leakage constant is higher, and the open-stopband behavior is completely eliminated, when comparing the unit cell with and without bias connection. As a result, gain of an LWA utilizing LC can be lowered, since besides higher material loss due to LC, more power is radiated at the first few unit cells. Since there is no way to provide bias to the unit cells without a bias line, a practical verification of this layout is not possible. Regardless, in order to be able to have a qualitative comparison in practice, the LWA with a pure Rexolite body (Fig. 2 top) serves as a non-tunable representation of the perpendicular alignment state, since the LC permittivity in perpendicular alignment and the one of Rexolite only differ by 0.07. In case of absence of LC (Rexolite only) the radiation elements can be directly placed on the DIL by metallizing and etching. However, in case of the LC filled antenna, a Pyralux foil of thickness 9 µm with the unit cell structure on top of it has to be glued on the DIL in order to seal the LC cavity.

The corresponding Brillouin Diagrams are plotted for the infinitely long LWAs consisting of Rexolite, Fig. 4(a), and for the LC LWA with both perpendicular, Fig. 4(b), and parallel, Fig. 4(c), LC alignment. We observe that due to the similarity in permittivity of Rexolite ($\varepsilon_r = 2.53$) and LC in perpendicular alignment ($\varepsilon_{r,\perp} = 2.46$) the Brillouin diagrams also show similarity, but the open-stopband is fully eliminated when including the bias line. If the LC is biased to its parallel alignment ($\varepsilon_{r,||} = 3.53$), the broadside frequency shifts to 79.3 GHz and the maximum frequency of operation without grating lobes is reduced to 97 GHz. This leads to an expected operational bandwidth of 22 GHz for the reconfigurable LWA, from 75 GHz to 97 GHz, defined by the smallest operational bandwidth, which is present in parallel LC alignment.

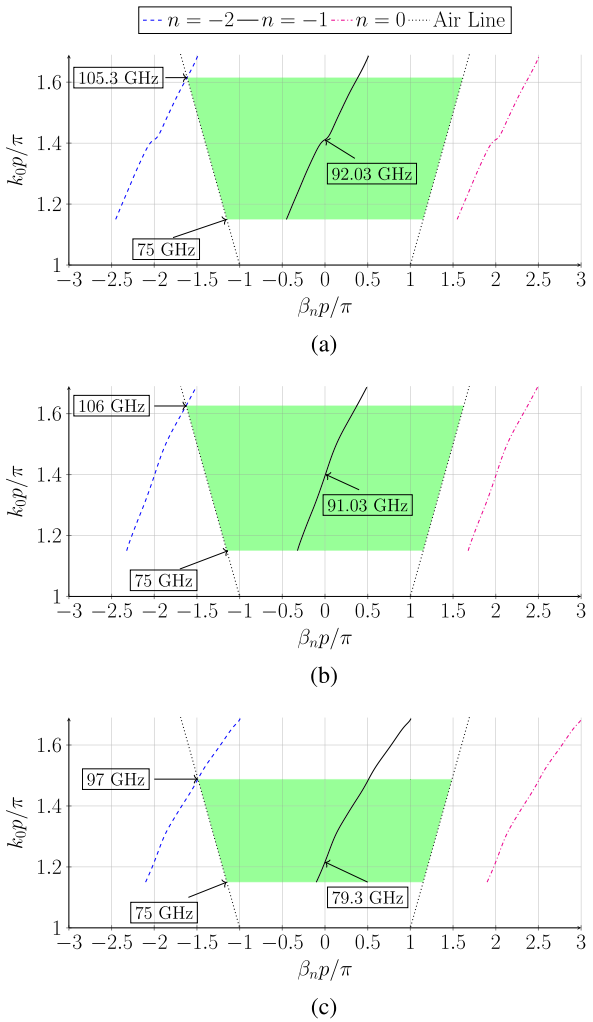

FIGURE 4. Calculated Brillouin diagrams of the structures introduced in Fig. 2 from 75 GHz to 110 GHz. The undisturbed frequency operation region is shaded in green. Beginning and end of this range in W-band as well as broadside frequency are indicated by markers. (a) Rexolite, isolated unit cells. (b) LC ($\varepsilon_{r,\perp} = 2.46$), connected unit cells. (c) LC ($\varepsilon_{r,\parallel} = 3.53$), connected unit cells.

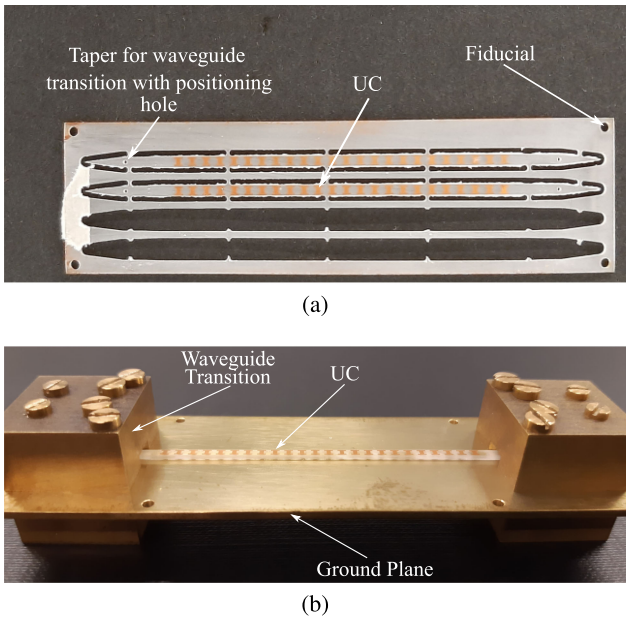

FIGURE 5. Fabrication of the non-reconfigurable LWA: (a) photolithografically structured Rexolite sheet from which the LWAs are cut; (b) LWA mounted on ground plane with WR10 to DIL transitions.

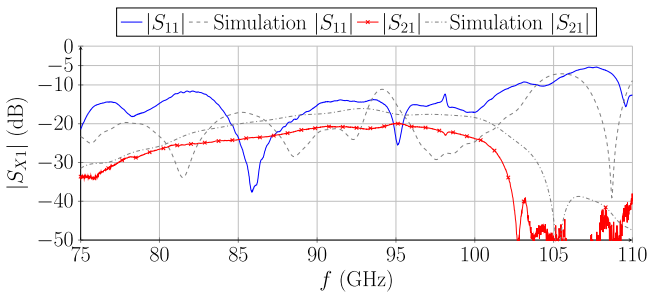

FIGURE 6. Matching and residual power of the non-reconfigurable LWA. Simulation model is according to Fig. 5(b).

IV. FABRICATION AND MEASUREMENT

A. NON-RECONFIGURABLE ANTENNA

In order to assess how fabrication of a finite structure influences the predicted radiation behavior, a demonstrator without LC is investigated first. It is realized by cutting the DIL of desired width $w = 1.8$ mm from a $d = 0.9$ mm thick Rexolite sheet, on which rows of $N = 24$ unit cells are photolithographically processed, resulting in a total antenna length of $N \cdot p = 55.2$ mm. During the photolithographic process, great care has to be taken, since Rexolite is very temperature sensitive and can start to deform. The antenna is glued on a ground plane with Rexolite adhesive. It has tapered ends in order to use WR10 to DIL transitions [10], which can be mounted on the ground plane, to feed the antenna and measure residual power at the end of the LWA. Fig. 5 depicts the metallized Rexolite sheet and the fully assembled LWA with two transitions. This setup is only used to determine matching and residual power, shown in Fig. 6. When antenna measurements are conducted, the second transition is replaced by absorber material in order to minimize reflections at the antenna's end, which can deteriorate the pattern. As visible in Fig. 6, the antenna is matched to up to 103 GHz and residual power drops at around 101 GHz. With a slight frequency shift, the measurement of the finite structure is in line with simulations and the corresponding Brillouin Diagram of the infinite structure (Fig. 4(a)). This shift is due to slightly increased height of the DIL caused by a glue layer thicker than anticipated in simulations. A comparison of simulated and measured patterns is given in Fig. 7. Especially at lower frequencies (backward radiation), side lobes are caused by small portions of power radiated from the waveguide transition to the forward region. From approximately 80 GHz on, the waveguide transition works optimally, and less power is radiated to the forward region. A typical fan beam of one-dimensional LWAs is

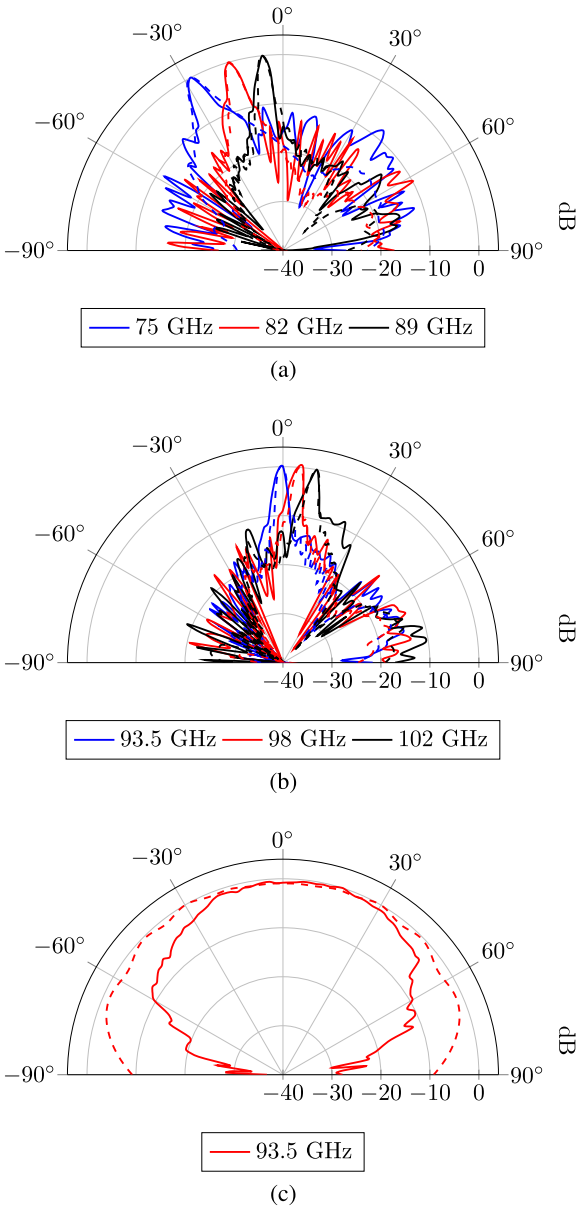

FIGURE 7. Normalized measured radiation patterns at selected frequencies. Simulated patterns are depicted with dashed lines. (a) E-plane, backward radiation (b) E-plane, broadside and forward radiation (c) H-plane at 93.5 GHz (broadside frequency).

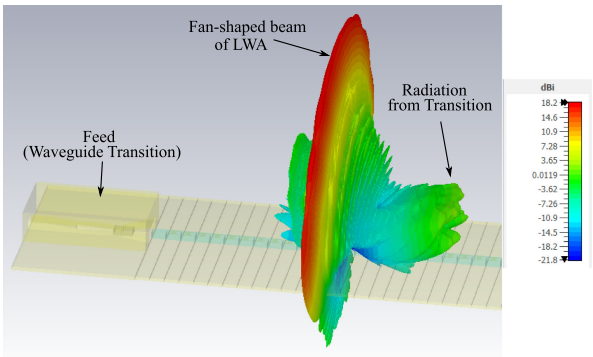

FIGURE 8. Simulated 3D radiation pattern of the LWA at 92 GHz with CST Studio Suite. The antenna model is transparent.

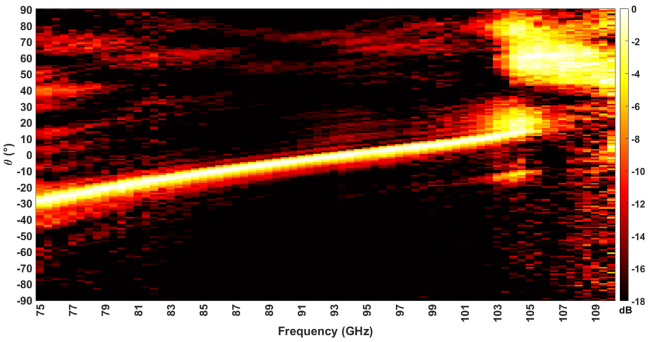

FIGURE 9. Heatmap of the normalized measured radiation characteristic in elevation plane of the non-reconfigurable Rexolite LWA.

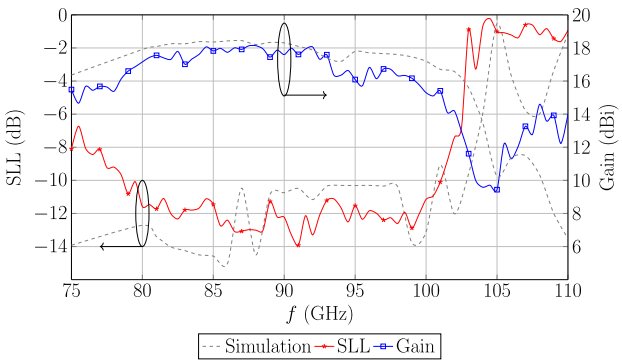

FIGURE 10. Measured gain and SLL of the Rexolite LWA.

present, i.e. in H-plane a wide pattern can be observed, while in E-plane the beam is narrow. Fig. 8 shows the simulated beam pattern at 92 GHz. Cross-polarization is below −20dB. Overall, a good agreement of simulation and measurement is observable, where deviations are mainly caused by the non-predictable final height of the glue layer beneath the antenna. The simulated radiation efficiency ranges between 93% and 87%, decreasing with frequency. The measured efficiency is 69% to 58%. Fig. 9 illustrates the elevation plane as a heatmap, showing that the antenna scans with 1.4°/GHz from −30° at 75 GHz through broadside to +10° at 102 GHz before the grating lobe phenomenon starts. The obtained gain and SLL over frequency are depicted in Fig. 10. From 80 GHz to 102GHz, the SLL is below −10 dB, and the gain remains stable in a range from 16 dBi to 18 dBi.

B. RECONFIGURABLE ANTENNA

Fabrication of the reconfigurable LC-LWA is similar to its non-reconfigurable counterpart in the previous section. A DIL with desired dimensions is cut from a Rexolite sheet, however, this sheet is not metallized, but has a cavity for LC hosting. It is tapered at its beginning, similar to [10], for better matching to the parallel tuning state. At the taper ends, there are small

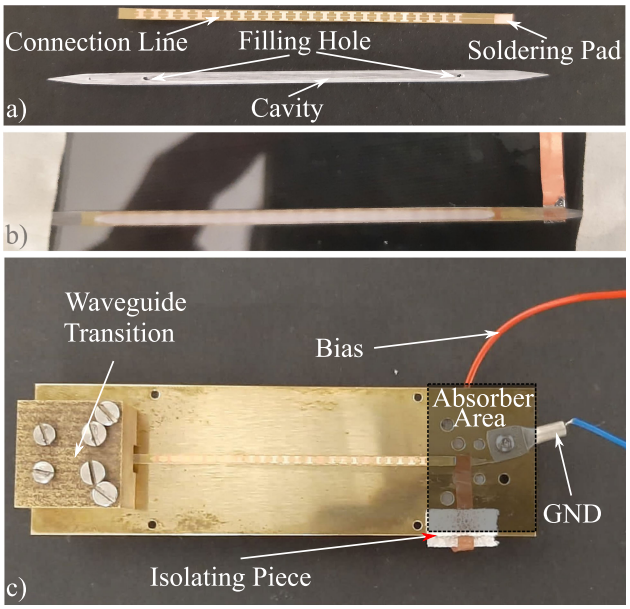

FIGURE 11. Assembly of the reconfigurable LC-LWA. (a) Rexolite body with filling holes and electrode structure on Pyralux are glued together to seal the cavity. (b) After LC injection, the LWA is glued on the ground plane. (c) The LWA is connected to bias and GND. For clarity, the necessary absorber is not shown in this picture, but the corresponding area occupied by the absorber material is highlighted.

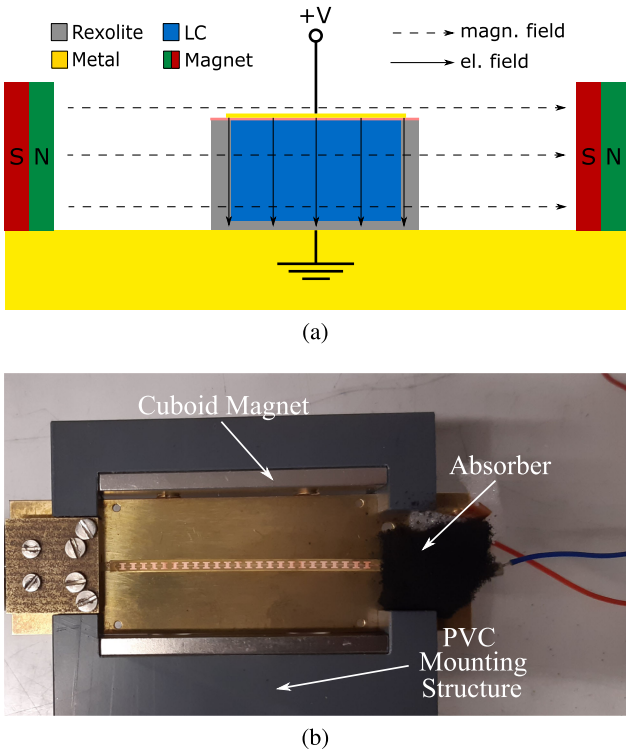

FIGURE 12. Hybrid bias of the reconfigurable LWA. (a) Hybrid bias concept. (b) Realization with cuboid magnets.

filling holes in the bottom of the DIL, see Fig. 11 a). The open-top side of the LC cavity is sealed by a 9 µm thin Pyralux foil, on which the electrode/unit cell structure is processed. For a direct comparison to the non-reconfigurable LWA, the same number of unit cells ($N = 24$) is used. Hence, the LC cavity is 55.2 mm long. Sealing is performed with the help of UV glue. After mounting of the Pyralux substrate, LC is injected through the filling holes with a syringe, and the filling holes are sealed with UV glue, shown in Fig. 11 b). The LWA is glued on the ground plane and the electrodes are connected to the bias supply, see Fig. 11 c). Bias is provided with means of a 1 kHz rectangular voltage signal with peak-to-peak voltage V_{pp}. Since electrodes and ground plane are isolated entities, no bias tee is necessary, and a small cable can be directly connected to the soldering pad on the Pyralux foil. In order to utilize the maximum amount of LC anisotropy and to show the capabilities of the antenna, a hybrid bias of electric and magnetic fields is employed in this first demonstrator. The principle is shown in Fig. 12. Without any bias voltage, the magnetic field assures perpendicular LC molecule alignment. With increasing voltage, both magnetic and electric field create intermediate molecule alignments until the electric field dominates and parallel LC molecule alignment is present. Due to the fact that the electrodes are directly mounted above the LC on the DIL, lower voltages of up to 50 V are required than those necessary for previously reported dielectric LC structures [7] of up to 300 V. Since a soldering point and a GND-clamp are present at the end of the antenna, no residual power can be measured, as these structures need to be

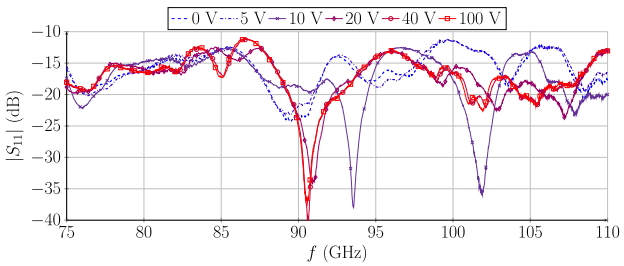

FIGURE 13. Measured magnitude of the reflection coefficient at different bias voltages V_{pp}.

carefully shielded by absorbing material. Fig. 13 displays $|S_{11}|$ at different bias voltages. Matching below −10 dB regardless of the used voltage is observed. Fig. 14 shows the measured E-plane as a heatmap for both 0 V and 50 V bias voltage. A frequency independent beam steering of the radiation behavior by $\Delta\theta \approx 10^\circ$ is achieved. Higher parasitic radiation from 75 GHz to 85 GHz than in Fig. 9 can be observed. This is due to the combination of the radiation of the waveguide transition and the high leakage constant, as seen in Fig. 3. This leads to SLLs between −5 dB to −10 dB in this range. Between 85 GHz to 100 GHz good SLL is achieved in all bias states. At higher frequencies, the SLL rises again. Fig. 15 shows measured patterns with different bias at lowest (85 GHz) and highest (100 GHz) frequency with tolerable SLL. Similar to the non-reconfigurable LWA, cross

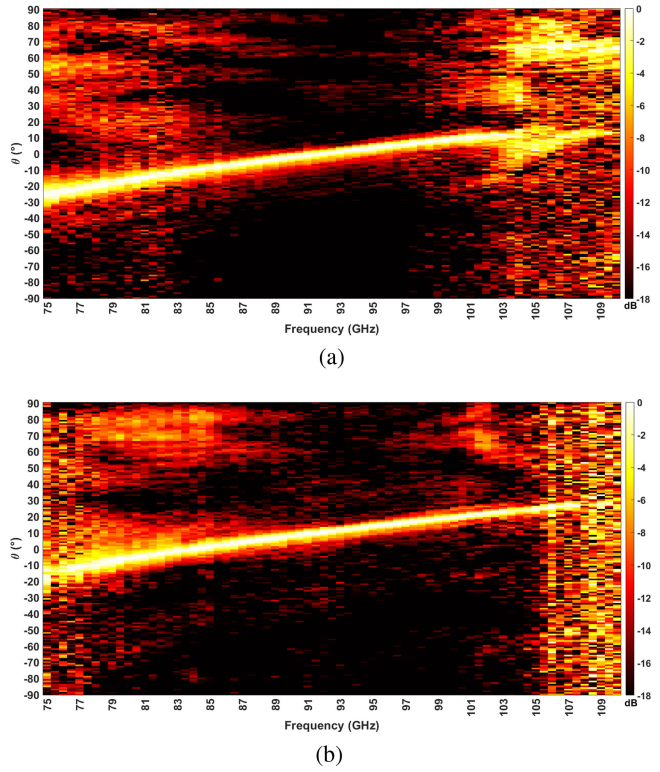

FIGURE 14. Heatmaps of the normalized measured radiation characteristic in elevation plane of the reconfigurable LWA at different bias voltages. The scanning behavior is shifted by 10 ° when changing from perpendicular to parallel LC orientation. Tolerable SLLs for both alignment states are achieved from 85 GHz to 100 GHz. (a) Perpendicular, 0 V bias. (b) Parallel, 50 V bias.

polarization is better than −20 dB in main beam direction. When comparing Fig. 15(a) and (b) it can be noted that the electrical scanning range $\Delta\theta$ is less compared to simulations. Instead of a simulated $\Delta\theta_{sim} = 15\,^\circ$ when changing LC permittivity from 2.46 to 3.53, about $\Delta\theta \approx 10^\circ$ is achieved in practice. By comparing the simulated achievable scanning range versus the measured one, we can estimate the available LC anisotropy in the antenna, as shown in Fig. 16. About 73% of the available material tuneability is obtained. The reason for this reduction is on the one hand from manufacturing tolerances along the LC cavity. On the other hand, a direct cause is the presence of a non-optimal bias field for parallel orientation, as the electrodes/unit cells and their bias line do not cover the whole LC volume. Since the LC volume is modelled uniformly along the LWA, effects at the corners of the bias structure are not included [41]. In addition, the anisotropy of LC at higher frequencies might be slightly less than given at 19 GHz, as hinted in [42], and assembly tolerances can lower the tuneable range. The correlation of electronically controlled scanning angle versus applied bias voltage is shown in Fig. 17. At 25 V to 30 V saturation in $\Delta\theta$ is achieved. Biasing with more than 50 V only leads to incremental increase in $\Delta\theta$, which are hardly recognized by the measurement setup.

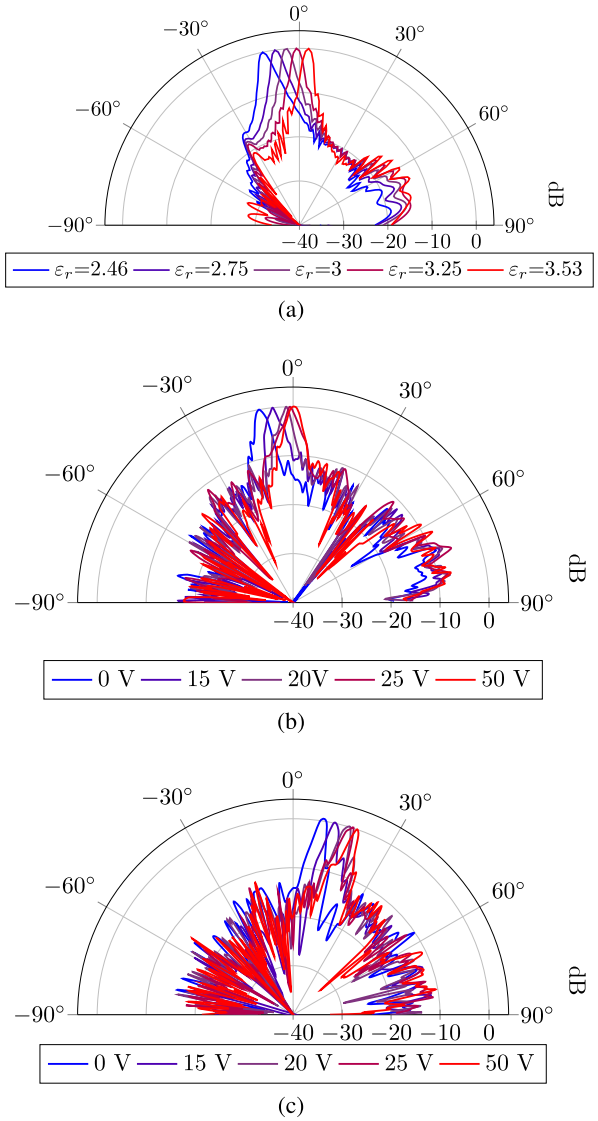

FIGURE 15. Measured patterns at beginning and end of the frequency range with tolerable SLL. For comparison, the simulated steering capabilities at 85 GHz are shown in (a). (a) Simulation at 85 GHz. (b) Measurement at 85 GHz. (c) Measurement at 100 GHz.

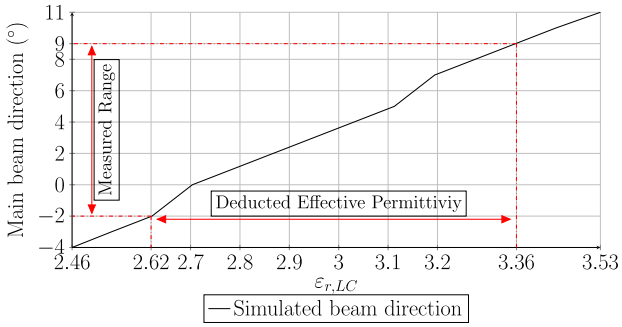

FIGURE 16. Deducted range of uniform LC permittivity when comparing simulated and measured steering angles at 91 GHz.

TABLE 2. Comparison of Different LC-LWAs. OSM: Open-Stopband Mitigation, SIW: Substrate Integrated Waveguide, GCPW: Grounded Coplanar Waveguide, FPC: Fabry-Perot Cavity. Values With an Asterisk (*) Are Extracted From Plots in the Corresponding Paper

Frequency range	Scanning range (f)	Scanning range (LC)	max. Gain	SLL	OSM	Topology	Measured	Ref.
around 10.1 GHz*	n.a.	120°	12.5 dBi*	< -11 dB*	n.a.	SIW	yes	[24]
11.85 - 12.55 GHz	40°	22°	4.5 dBi	> -10 dB	no	Microstrip	yes	[25]
26 - 30 GHz*	100°*	11°	n.a.	> -10 dB*	no	Microstrip	yes	[26]
37 - 43 GHz	75°*	35°*	$D = 18$ dBi*	-18 dB	yes	GCPW	no	[28]
around 0.56 THz	n.a.	20°	$D = 15.52$ dBi	-5 dB*	yes	FPC	no	[27]
85 - 102 GHz	40°	10°	15 dBi	< -10 dB	yes	DIL	yes	This

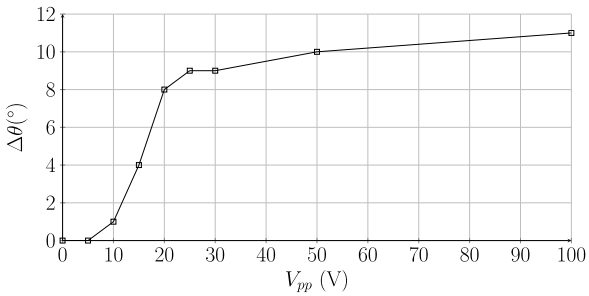

FIGURE 17. Measured scanning range in dependency of bias voltage at 91 GHz.

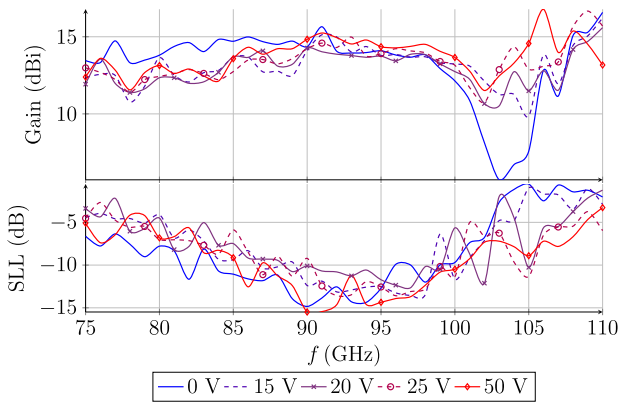

FIGURE 18. Measured gain (top) and SLL (bottom) of the reconfigurable LC-LWA at different frequencies.

Gain and SLL are shown in Fig. 18. Gain is showing stable behavior in a range of 12 dBi to 15 dBi and is especially constant from 90 GHz to 100 GHz. SLL is below -8 dB, starting after 85 GHz for each permittivity, and is below -10 dB from 90 GHz to 100 GHz. It begins to rise again at around 100 GHz. The simulated radiation efficiency ranges between 85% and 55%, decreasing with frequency. The measured efficiency is 69% to 42%.

V. CONCLUSION AND OUTLOOK

This paper presents a reconfigurable dielectric image line leaky wave antenna operating with liquid crystal. For the first time, the bias network is deliberately treated as part of the dielectric antenna, opposed to previous applications where LC is combined with dielectric waveguides. In contrast to many existing LC-LWA papers, this approach is investigated both theoretically and practically. In order to do so, a DIL-LWA without LC is realized and compared to the LC antenna, revealing practical limitations and challenges of the design. All demonstrators can scan through broadside, hence they mitigate the open-stopband. The non-reconfigurable LWA is easy to fabricate, and shows high gain of up to 18 dBi, while keeping an SLL below -10 dB in most of its designed operation region. It scans its beam from $-30°$ to $+10°$ with an operating frequency change from 75 GHz to 102 GHz, and is a suitable antenna for mmW applications in W-Band. The reconfigurable LC-LWA can turn its whole scanning sector by 10°. Due to the proximity of bias electrodes to the LC volume, fairly low bias voltages of maximally ± 25 V can be used. In comparison to fully dielectric LC phased arrays [7] fabrication of the antenna is very simple, as only one LC cavity is present instead of many. As a result, solely one voltage is directly linked to a steering angle, and hence antenna characterization in an embedded environment can be done easily. In order to enhance this antenna, the fabrication by hand and the use of glue have to be avoided. A promising alternative can be 3D printing. A DIL with a cavity, metallized with bias electrodes, can be printed on the top layer of any PCB, regardless of other, conventional waveguides or components elsewhere on it. This omits the conventional approach of costly and complex LC cavities in the PCB layout. In order to optimize the tuning efficiency, different metallic shapes, most importantly of the connection line, can be used to achieve higher parallel alignment of the LC. The use of magnets for better perpendicular alignment could be avoided if experimental LC mixtures containing polyacrylonitrile nanofibers [43] are employed. A translation of the LC-LWA to the terahertz regime is possible, if smaller cavities can be handled, providing higher absolute bandwidths, and lowering the necessary bias voltages due to the lower DIL height. Table 2 compares this work to different LC-LWAs. Especially at comparable higher mmW-frequencies, no LC-LWA has been realized and measured so far.

ACKNOWLEDGMENT

The authors would like to thank Merck KGaA, Darmstadt, Germany for the supply of liquid crystal, and Peter Kießlich for his assistance with the photolithographic processes.

REFERENCES

[1] G. Oliveri, D. H. Werner, and A. Massa, "Reconfigurable electromagnetics through metamaterials–A review," *Proc. IEEE*, vol. 103, no. 7, pp. 1034–1056, Jul. 2015.

[2] S. K. Koul and S. Dey, "K-band 4-bit phase shifter using two back to back MEMS SP16T switching networks," *J. Microelectromech. Syst.*, vol. 27, no. 4, pp. 643–655, Aug. 2018.

[3] J. J. Venter and T. Stander, "W-band capacitively loaded slow-wave transmission line phase shifter in 130 nm CMOS," in *Proc. IEEE AFRICON*, 2017, pp. 555–558.

[4] A. Tagantsev, V. Sherman, K. Astafiev, J. Venkatesh, and N. Setter, "Ferroelectric materials for microwave tunable applications," *J. Electroceramics*, vol. 11, no. 1/2, pp. 5–66, Sep. 2003.

[5] P. Bao, T. J. Jackson, X. Wang, and M. J. Lancaster, "Barium strontium titanate thin film varactors for room-temperature microwave device applications," *J. Phys. D, Appl. Phys.*, vol. 41, no. 6, Feb. 2008, Art. no. 063001.

[6] H. Maune, M. Jost, R. Reese, E. Polat, M. Nickel, and R. Jakoby, "Microwave liquid crystal technology," *Crystals*, vol. 8, no. 9, Sep. 2018, Art. no. 355.

[7] E. Polat *et al.*, "Reconfigurable millimeter-wave components based on liquid crystal technology for smart applications," *Crystals*, vol. 10, no. 5, Apr. 2020, Art. no. 346.

[8] D. King and S. Schlesinger, "Dielectric image lines," *IEEE Trans. Microw. Theory Techn.*, vol. 6, no. 3, pp. 291–299, Jul. 1958.

[9] S. Schlesinger and A. Vigants, "Experimental comparison of image line radiators and polyrod antennas," *IRE Trans. Antennas Propag.*, vol. 8, no. 5, pp. 521–522, Sep. 1960.

[10] H. Tesmer, R. Reese, E. Polat, R. Jakoby, and H. Maune, "Dielectric image line liquid crystal phase shifter at W-band," in *Proc. German Microw. Conf.*, 2020, pp. 156–159.

[11] T. Itoh, "Application of gratings in a dielectric waveguide for leaky-wave antennas and band-reject filters (short papers)," *IEEE Trans. Microw. Theory Techn.*, vol. 25, no. 12, pp. 1134–1138, Dec. 1977.

[12] F. Monticone and A. Alu, "Leaky-wave theory, techniques, and applications: From microwaves to visible frequencies," *Proc. IEEE*, vol. 103, no. 5, pp. 793–821, May 2015.

[13] M. Memarian and G. V. Eleftheriades, "Dirac leaky-wave antennas for continuous beam scanning from photonic crystals," *Nature Commun.*, vol. 6, no. 1, pp. 1–9, Jan. 2015.

[14] J. H. Choi and T. Itoh, "Beam-scanning leaky-wave antennas," in *Handbook of Antenna Technologies*. Singapore: Springer-Verlag, 2016, pp. 1697–1735.

[15] M. Geiger, M. Hitzler, and C. Waldschmidt, "A flexible dielectric leaky-wave antenna at 160 GHz," in *Proc. 47th Eur. Microw. Conf*, 2017, pp. 240–243.

[16] C. S. Prasad and A. Biswas, "Dielectric image line-based leaky-wave antenna for wide range of beam scanning through broadside," *IEEE Trans. Antennas Propag.*, vol. 65, no. 8, pp. 4311–4315, Aug. 2017.

[17] K. Wu, Y. J. Cheng, T. Djerafi, and W. Hong, "Substrate-integrated millimeter-wave and terahertz antenna technology," *Proc. IEEE*, vol. 100, no. 7, pp. 2219–2232, Jul. 2012.

[18] S. Paulotto, P. Baccarelli, F. Frezza, and D. R. Jackson, "A novel technique for open-stopband suppression in 1-D periodic printed leaky-wave antennas," *IEEE Trans. Antennas Propag.*, vol. 57, no. 7, pp. 1894–1906, Jul. 2009.

[19] S. Otto, A. Al-Bassam, A. Rennings, K. Solbach, and C. Caloz, "Transversal asymmetry in periodic leaky-wave antennas for bloch impedance and radiation efficiency equalization through broadside," *IEEE Trans. Antennas Propag.*, vol. 62, no. 10, pp. 5037–5054, Oct. 2014.

[20] C. S. Prasad, A. Biswas, and M. J. Akhtar, "Leaky wave antenna for wide range of beam scanning through broadside in dielectric image line environment," *Microw. Opt. Technol. Lett.*, vol. 60, no. 7, pp. 1707–1713, May 2018.

[21] Y.-L. Lyu, F.-Y. Meng, G.-H. Yang, Q. Wu, and K. Wu, "Leaky-wave antenna with alternately loaded complementary radiation elements," *IEEE Antennas Wireless Propag. Lett.*, vol. 17, no. 4, pp. 679–683, Apr. 2018.

[22] J. Liu, W. Zhou, and Y. Long, "A simple technique for open-stopband suppression in periodic leaky-wave antennas using two nonidentical elements per unit cell," *IEEE Trans. Antennas Propag.*, vol. 66, no. 6, pp. 2741–2751, Jun. 2018.

[23] N. Javanbakht, B. Syrett, R. E. Amaya, and J. Shaker, "A review of reconfigurable leaky-wave antennas," *IEEE Access*, vol. 9, pp. 94 224–94 238, 2021.

[24] H. Kim and S. Nam, "Performance improvement of LC-based beam steering leaky wave holographic antenna using decoupling structure," *IEEE Trans. Antennas Propag.*, vol. 70, no. 4, pp. 2431–2438, Apr. 2022.

[25] S. Ma, P.-Y. Wang, F.-Y. Meng, J.-H. Fu, and Q. Wu, "Electronically controlled beam steering leaky wave antenna in nematic liquid crystal technology," *Int. J. RF Microw. Comput.-Aided Eng.*, vol. 30, no. 6, Feb. 2020, Art. no. e22188.

[26] M. Roig, M. Maasch, C. Damm, O. H. Karabey, and R. Jakoby, "Liquid crystal based tunable composite right/left-handed leaky-wave antenna for Ka-band applications," in *Proc. Eur. Microw. Conf.*, 2013, pp. 759–762.

[27] W. Fuscaldo *et al.*, "Tunable Fabry–Perot cavity THz antenna based on leaky-wave propagation in nematic liquid crystals," *IEEE Antennas Wireless Propag. Lett.*, vol. 16, pp. 2046–2049, 2017.

[28] S. Foo, "Electronically steerable, low-sidelobe, CRLH-metamaterial leaky-wave antenna," in *Proc. 13th Eur. Conf. Antennas Propag.*, 2019, pp. 1–4.

[29] D. R. Jackson and A. A. Oliner, "Leaky-wave antennas," in *Modern Antenna Handbook*, Hoboken, NJ, USA: Wiley, Nov. 2007, pp. 325–367.

[30] K. Solbach and I. Wolff, "Dielectric image line groove antennas for millimeter waves, Part II: Experimental verification," *IEEE Trans. Antennas Propag.*, vol. 33, no. 7, pp. 697–706, Jul. 1985.

[31] A. Patrovsky and K. Wu, "Substrate integrated image guide array antenna for the upper millimeter-wave spectrum," *IEEE Trans. Antennas Propag.*, vol. 55, no. 11, pp. 2994–3001, Nov. 2007.

[32] A. S. Al-Zoubi, A. A. Kishk, and A. W. Glisson, "Aperture coupled rectangular dielectric resonator antenna array fed by dielectric image guide," *IEEE Trans. Antennas Propag.*, vol. 57, no. 8, pp. 2252–2259, Aug. 2009.

[33] H. Chen, M. Neshat, S. Gigoyan, D. Saeedkia, and S. Safavi-Naeini, "A frequency agile beam steerable tapered dielectric image-line antenna array with novel feeding structure," in *Proc. IEEE Radio Wireless Symp.*, 2009, pp. 147–150.

[34] J. Xing, L. Quan, L. Xiaofeng, L. Xin, and W. Kun, "A 77GHz dielectric resonator antenna array using dielectric image insular guide," in *Proc. 6th Asia-Pacific Conf. Antennas Propag.*, 2017, pp. 1–3.

[35] Y. Torabi, G. Dadashzadeh, M. Hadeie, H. Oraizi, and A. Lalbakhsh, "A wide-angle scanning sub-terahertz leaky-wave antenna based on a multilayer dielectric image waveguide," *Electronics*, vol. 10, no. 17, 2021, Art. no. 2172. [Online]. Available: https://www.mdpi.com/2079-9292/10/17/2172

[36] P. Bhartia, *Millimeter Wave Engineering and Applications*. New York, NY, USA: Wiley, 1984.

[37] G. Friedsam and E. Biebl, "Precision free-space measurements of complex permittivity of polymers in the W-band," in *IEEE MTT-S Int. Microw. Symp. Dig.*, 1997, vol. 3, pp. 1351–1354 .

[38] M. Guglielmi and G. Boccalone, "A novel theory for dielectric-inset waveguide leaky-wave antennas," *IEEE Trans. Antennas Propag.*, vol. 39, no. 4, pp. 497–504, Apr. 1991.

[39] M. Wittek, C. Fritzsch, and D. Schroth, "Employing liquid crystal-based smart antennas for satellite and terrestrial communication," *Inf. Display*, vol. 37, no. 1, pp. 17–22, Jan. 2021.

[40] Y.-L. Lyu *et al.*, "Leaky-wave antennas based on noncutoff substrate integrated waveguide supporting beam scanning from backward to forward," *IEEE Trans. Antennas Propag.*, vol. 64, no. 6, pp. 2155–2164, Jun. 2016.

[41] D. C. Zografopoulos and R. Beccherelli, "Tunable terahertz fishnet metamaterials based on thin nematic liquid crystal layers for fast switching," *Sci. Rep.*, vol. 5, no. 1, pp. 1–11, Aug. 2015.
[42] E. Polat *et al.*, "Characterization of liquid crystals using a temperature-controlled 60 GHz resonator," in *Proc. IEEE MTT-S Int. Microw. Workshop Ser. Adv. Mater. Processes RF THz Appl.*, 2019, pp. 19–21.
[43] T. N. Lang, V. B. Bui, Y. Inoue, and H. Moritake, "Response improvement of liquid crystal-loaded NRD waveguide type terahertz variable phase shifter," *Crystals*, vol. 10, no. 4, Apr. 2020, Art. no. 307.

HENNING TESMER was born in Kassel, Germany, in 1992. He received the B.Sc. and M.Sc. degrees from Technische Universität Darmstadt, Darmstadt, Germany, in 2015 and 2018, respectively, where he is currently working toward the Ph.D. degree with the Institute of Microwave Engineering and Photonics. His research interests include liquid crystal-based tunable dielectric waveguides and components for millimeter-wave applications.

RANI RAZZOUK was born in Tartous, Syria, in 1990. He received the B.Sc. degree in electrical engineering from Al-Baath University, Homs, Syria, in 2015, and the M.Sc. degree in electrical engineering from Technische Universität Darmstadt, Darmstadt, Germany, in October 2021. This work was based on the results of his master's thesis. He is currently employed as a EMF Manager with DFMG Deutsche Funkturm GmbH, Frankfurt, Germany.

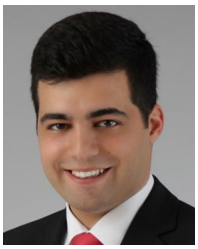

ERSIN POLAT was born in Alzenau, Germany, in 1991. He received the B.Sc. and M.Sc. degrees in electrical engineering and information theory from Technische Universität Darmstadt, Darmstadt, Germany, in 2014 and 2017, respectively, where he is currently working toward the Ph.D. degree with Microwave Engineering Group. His research interests include tunable microwave filters based on liquid crystal technology and material characterization.

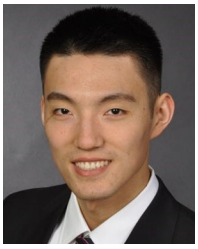

DONGWEI WANG (Graduate Student Member, IEEE) was born in Taiyuan, China, in 1991. He received the B.Eng. degree from Zhejiang University, Hangzhou, China, and the M.Sc. degree from the Karlsruher Institut für Technologie, Karlsruhe, Germany. He is currently working toward the Ph.D. degree with the Institute of Microwave Engineering and Photonics, Technische Universität Darmstadt, Darmstadt, Germany. His research focuses on liquid crystal-based tunable planar devices with slow-wave effect.

ROLF JAKOBY (Member, IEEE) was born in Kinheim, Germany, in 1958. He received the Diploma-Ing. and Doctorate-Ing. degrees in electrical engineering from the University of Siegen, Siegen, Germany, in 1985 and 1990, respectively. In 1991, he joined the Research Center of Deutsche Telekom, Darmstadt, Germany. Since 1997, he has been a Full Professor of microwave engineering with Technische Universität Darmstadt, Darmstadt, Germany. He is currently a Co-Founder of ALCAN Systems GmbH, a smart antenna company. He is the author of more than 599 publications, which include 161 in journals, and holds more than 23 patents. His research interests include chipless RFID sensor tags, biomedical sensors and applicators and also tunable passive microwave devices and beamsteering antennas, using electromagnetic bandgap structures, ferroelectric, and liquid crystal technologies. He was the recipient of the Award from CCI Siegen for his excellent Ph.D. in 1992 and ITG-Prize in 1997 for an excellent publication in IEEE Transactions on Antennas and Propagation. His group was the recipient of 24 awards and prizes for best papers and doctoral dissertations. He is the Editor-in-Chief of FREQUENZ, DeGruyter, a member of VDE/ITG and IEEE/MTT/AP societies. He was the Chairman of EuMC in 2007 and GeMiC in 2011, and Treasurer of EuMW in 2013 and 2017, respectively.